M&C 2001 Salt Lake City, Utah, USA, September 2001.

PAPER TITLE

Uncontrolled Rod Bank Withdrawal Benchmark Analyses with CORETRAN and RETRAN-3D

Hakim Ferroukhi and Paul Coddington
Paul Scherrer Institut
CH-5232 Villigen, Switzerland
Hakim.Ferroukhi@psi.ch , Paul.Coddington@psi.ch

Keywords: CORETRAN/RETRAN-3D, 3-D Kinetics, Reactivity Transients, Control Rod Model, Thermal-Hydraulic Channel Grouping

ABSTRACT

The benchmark on uncontrolled rod bank withdrawal at hot-zero-power, organized by the OECD/NEA, has been analysed with the three-dimensional kinetic codes CORETRAN and RETRAN-3D. This analysis is part of a systematic assessment of these codes against past present and future international benchmarks. The goal is to develop a methodology for the transient analysis of the Swiss LWRs, based on a coupling in which the core simulator CORETRAN is used to generate the initial boundary conditions for a RETRAN-3D core/thermal-hydraulic system analysis. Two of the transient cases included in the benchmark have been analysed with both CORETRAN and RETRAN-3D to verify the consistency between both codes' neutronic solutions. The results of the analysis show that, both from a steady-state and a transient point of view, the consistency is verified, providing confidence in the use of these codes in a coupled manner. Compared to the previous benchmark solutions, both CORETRAN and RETRAN-3D predict a power excursion delayed by around 2 s. The magnitude of the power peak and the injected enthalpy are significantly affected by this delay. An investigation has shown that the results are due to a linear interpolation of the cross-section for partially inserted rods. In addition, by analysing these transients, it is found that a grouping of the thermal-hydraulic channels, usually necessary in best-estimate codes such as RETRAN-3D, is more likely to affect the results for slow reactivity transients, compared to fast transients, since the development of the transient depends more on the global behaviour of the core.

1. INTRODUCTION

At PSI, one objective is to implement the 3-D kinetic simulators CORETRAN/RETRAN-3D in a computer code environment that will allow a wide range of 3-D transient analyses for the Swiss LWRs to be performed. CORETRAN is a full 2-group 3-D static core simulator and kinetic code which can be used both in a steady-state depletion mode and in a transient mode for core-only analyses. RETRAN-3D is a 2-group transient analysis code intended for best-estimate coupled 3-D core/thermal-hydraulic

system transients. One feature of the codes is that they can be linked so that the initial boundary conditions for a RETRAN-3D analysis, including core geometry data and 3-D instantaneous cross-sections dependencies, are generated by a CORETRAN static calculation. This procedure is possible since both codes use the same neutronic numerical algorithm. One aspect that differs between the codes is that a full thermal-hydraulic core representation is used in CORETRAN while a grouping of the thermal-hydraulic (T/H) channels, referred to in this paper as the channel lumping, may be used where necessary, for RETRAN-3D best-estimate plant system analyses of large LWR models. Therefore, the analysis of the OECD/NEA core reactivity transient benchmarks is not only intended to assess the codes neutronic solutions by comparing to other 3-D solutions but also to verify the consistency between CORETRAN and RETRAN-3D as well as to identify modelling options, such as the T/H channel lumping, that must be considered with care when analysing these types of transients.

2 OECD/NEA PWR REACTIVITY INITIATED TRANSIENTS

The first benchmark that was analysed with CORETRAN and RETRAN-3D as part of this assessment was the PWR rod ejection analysis at hot-zero and full–power conditions. For this type of fast transients, it was found that a full core CORETRAN model and a 37-T/H channel RETRAN-3D lumped model would give very similar results, which were moreover in excellent agreement with the benchmark reference solution (Ferroukhi, 2001a, 2001b)

The second OECD/NEA benchmark, reported in this paper, concerns slow reactivity transients initiated by an uncontrolled withdrawal of rod banks at hot-zero-power (HZP) and presented in (Fraikin, 1997). Since the nature of the transients is significantly different compared to the first benchmark, it was considered appropriate to also analyse this benchmark with CORETRAN and RETRAN-3D.

3. UNCONTROLLED ROD BANKS WITHDRAWAL AT HZP

3.1 Benchmark Specification

For this second benchmark, the same hypothetical core as for the rod ejection benchmark (Finnemann, 1992) is used. Moreover, most of the specifications, including neutron modelling and fuel thermophysical properties, remained unchanged. One difference to note, however, is that in the first benchmark, a linear interpolation of the cross-sections with respect to the nodal control rod insertion was specified, while for this second benchmark the use of a more advanced model, if available, was recommended. This model is referred to as the dynamic control rod model (DCRM) in this paper. Since the current versions of CORETRAN and RETRAN-3D use a linear DCRM, such model is also used for the analysis of this second benchmark. However, a sensitivity study as a function of different DCRM models is included as part of this analysis.

3.2 Transient Cases

In the original benchmark, four different transient cases were defined. In this paper, two of these cases, labelled case B and case D (same notation as in (Fraikin, 1993))

are analysed with CORETRAN/RETRAN-3D. Theses cases were selected because they had the highest reactivity worth. The same initial control rod pattern and operating conditions are used in both cases, making them identical from a steady-state point of view. From a transient point of view, case B is characterised by the withdrawal of rod banks 2 and 3, as shown in Fig. 1 for the upper right core quadrant (noting that the core is characterised by a ¼ rotational symmetry). In case D, rod banks 1 and 2 are withdrawn as shown in Fig. 2. The reactivity worth is higher in case B (around 3900 pcm compared to 3200 pcm in case D) and the reactivity insertion occurs both at the core periphery and in the central core region. In case D, the reactivity insertion occurs towards the core peripheral zone. In both cases, the banks are initially fully inserted and the withdrawal speed is v =1.91 cm/s

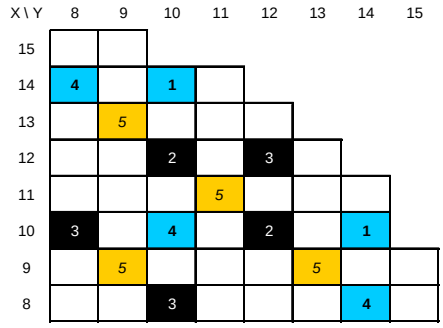

Fig 1. Case B - Control Rod Banks

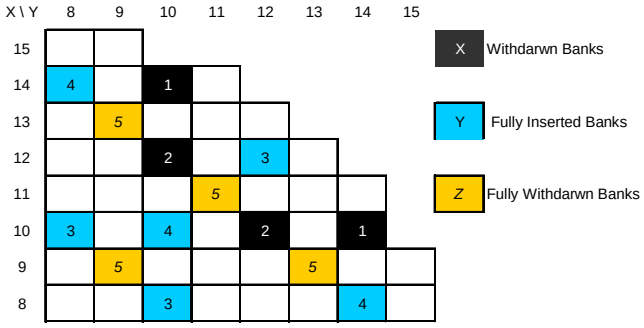

Fig.2 Case D – Control Rod Banks

The initial steady-state radial power distribution, identical in both cases, is shown in Fig.3.

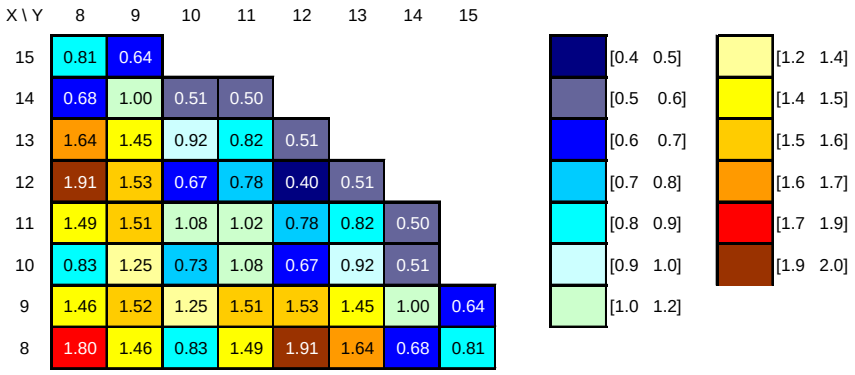

Fig 3. Case B / D – Steady-State Radial Power Distribution (Radial Factors)

3.3 CORETRAN / RETRAN-3D Models

The same CORETRAN / RETRAN-3D neutronic algorithm as in (Ferroukhi, 2001a/b) is used for the analyses here. It is based on a transverse-integrated nodal method using the Analytical Nodalization Method (Smith, 1979) and quadratic polynomials to describe the transverse leakage (Bennewitz, 1975). A theta-differencing scheme is used

for the temporal discretization of both the neutron flux (fully implicit) and the precursor equation (central difference). This neutronic model is identical to the one used by the original ARROTTA code (Eisenhart, 1991).

In both CORETRAN and RETRAN-3D, the neutronic representation of the fuel assemblies uses a 2x2 radial mesh and 16 axial heated nodes. From a thermal-hydraulic point of view, all fuel assemblies are represented as single individual and separated (i.e. cross-flow neglected) flow channels with a 1x1 radial mesh. In CORETRAN, a full core model is used while the RETRAN-3D calculations are performed taking advantage of the ¼ core symmetry.

4 STEADY-STATE RESULTS

A summary of the steady-state results obtained with both codes for cases B and D is given in Table 1. The table shows the critical boron concentration, the core average axial (Fax) peaking factors, the radial peaking factor for the core (Frad) and for axial layers 6 (Frad(6)) and 13 (Frad(13)) and finally, the nodal peaking factor (ppf). For all these results, the deviation from the benchmark reference solution is given. In addition, the standard deviation (STD) of the previous solutions is specified.

Table 1 – Summary of Steady-State Results for Case B and D

Case		Boron (ppm)	Fax	Frad	Frad(6)	Frad(13)	ppf
B/D	**Reference**	**793.6**	**1.507**	**1.912**	**2.377**	**1.245**	**2.886**
	CORETRAN	+5.2	+0.002	-0.001	+0.001	-0.003	0.000
	RETRAN-3D	+5.4	+0.003	0.000	+0.001	-0.004	0.000
	Previous Solutions STD	*6.6*	*0.004*	*0.007*	*0.007*	*0.008*	*0.108*

As can be seen, the CORETRAN and RETRAN-3D results, similar to the previous solutions, are very close to the reference solution. The same observation was also made for the previous benchmark (Ferroukhi, 2001a). This is in a sense to be expected since the thermal-hydraulic feedback variables are at HZP uniform across the core and this therefore eliminates the T/H effects on the neutronic solution. If the results are looked at in detail, it can be seen that CORETRAN and RETRAN-3D predict a slightly larger boron concentration than the reference solution. One probable reason is that a finer neutronic mesh is used in the reference solution (3x3 radial, 48 axial) and that CORETRAN/RETRAN-3D tend to predict a slightly increased core reactivity with coarser neutronic mesh sizes (Ferroukhi, 2001c). Concerning the 3-D power distribution, the peaking factors in Table 1 show that it is well captured by both CORETRAN and RETRAN-3D. The peaking factors indicate though that the axial power shape is slightly more bottom-peaked in these two codes compared to the reference solution. Finally, the consistency between CORETRAN and RETRAN-3D provides confidence in using the PSI methodology where a CORETRAN static calculation produces the input data (i.e. cross-section dependencies and core geometrical data) for a subsequent RETRAN-3D analysis.

5 TRANSIENT RESULTS

5.1 Dynamic Control Rod Model

In this section, the transient results for cases B and D are presented. As mentioned previously, the CORETRAN and RETRAN-3D current DCRM uses a linear interpolation of the cross-sections with respect to the control rod insertion within an axial node:

$$\Sigma = p \cdot \Sigma_C + (1-p) \cdot \Sigma_U \tag{1}$$

The nominal transient results with CORETRAN and RETRAN-3D obtained with this model are labelled with the index "I" in the following discussion. However, because the specification for this benchmark was to use a more advanced DCRM model if available, it was found appropriate to assess the impact of the DCRM model on the results. To do so, a non-linear DCRM similar to the one used in the RAMONA-3 code (Scandpower, 1996) was implemented in CORETRAN/ RETRAN-3D and the transient cases B and D were thereafter re-analysed using this DCRM. Such model was selected as an example to demonstrate how a non-linear interpolation of the cross-sections for partially controlled nodes affect the results for slow reactivity transient analysis. Hence, the non-linear DCRM used here as a sensitivity study has the following form and is applied to all cross-sections:

$$\Sigma = f(p) \cdot \Sigma_C + [1 - f(p)] \cdot \Sigma_U \tag{2a}$$

where

$$f(p) = \frac{b \cdot p}{1 + b - p} \text{ and } 0.5 \le b \le 1 \tag{2b}$$

In this paper, the additional CORETRAN/RETRAN-3D calculations with the above non-linear DCRM, labelled with the index "II" in the following sections, are performed using b=1.0 in Eq. 2b. However, other choices of b were investigated in (Ferroukhi, 2001c) and confirmed the conclusions that are obtained here when the results using a non-linear DCRM with b=1.0 are compared to the results using a linear DCRM.

In order to illustrate how a non-linear model, such as given by Eq. (2a,b), affects the reactivity increase within a node compared to a linear model, the change in the thermal fission-to-absorption cross-section ratio as function of the node insertion is shown in Fig. 4a for one of the specified nodal nuclear data sets. In Fig. 4b, the corresponding change in thermal fission-to-absorption ratio if the axial node height is reduced by a factor of 2 is shown.

As can be seen in both these figures, for a given partial insertion, the ratio is larger with a non-linear model and increases as the model is made increasingly non-linear (i.e. smaller values of b).

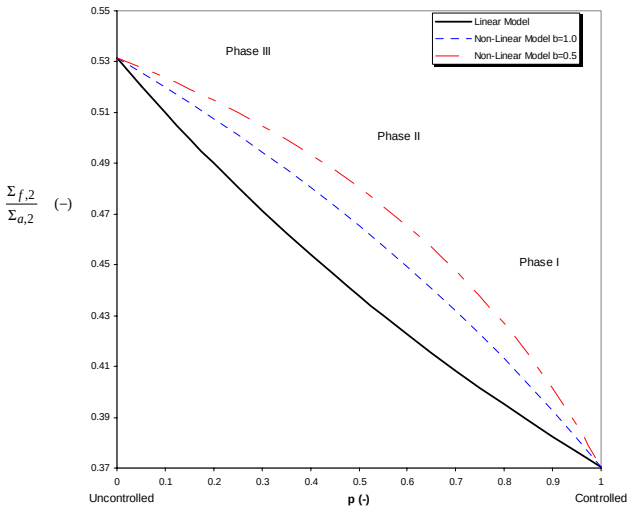

Fig. 4a Thermal Fission-to-Absorption Ratio as function of DCRM

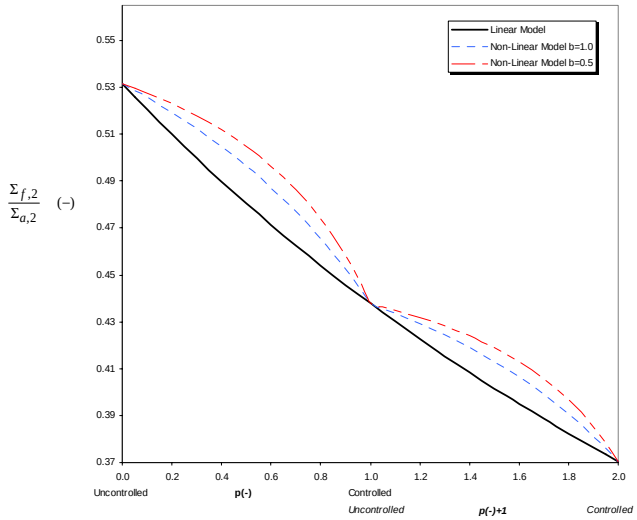

Fig. 4b Thermal Fission-to-Absorption with node height reduced by 50%

Based on Fig. 4a, the difference in reactivity insertion rate, assumed here to be represented by the increase in the rate of the thermal fission-to-absorption ratio, between the different DCRM models can be divided into three phases. When the node is nearly fully controlled, shown as Phase I in Fig 4a, the reactivity insertion rate is larger when an increasingly non-linear DCRM is used. In Phase II, i.e. when the partial insertion p is around 0.5, all models give a similar reactivity insertion rate. In Phase III, when the nodal insertion approaches the fully uncontrolled state, the reactivity rate becomes smaller for non-linear models when compared to a linear model.

Finally, when comparing Fig. 4a and Fig. 4b, it is seen that when the axial node height is reduced, the differences between different DCRM are reduced. So that if the axial node height is sufficiently small, the difference will eventually be eliminated.

5.2 CORETRAN / RETRAN Transient Results

The transient reactor power calculated by CORETRAN and RETRAN-3D is shown for case B in Fig.5. Results obtained with the linear “nominal” CORETRAN /RETRAN-3D DCRM (Eq. (1)) and with a non-linear DCRM model (Eq. (2) with b=1) are presented.

As shown by Fig. 5, CORETRAN and RETRAN-3D give nearly identical results. This can be seen clearly for the calculations using the linear model (I) while with the non-linear model (labelled II), although the resolution of the figure does not clearly show it, the CORETRAN and RETRAN-3D solutions are also very close to each other.

However, compared to the other solutions, it is also clearly seen that when using a linear DCRM, the predicted power excursion occurs around 2 s later than most other solutions and the peak magnitude is significantly smaller.

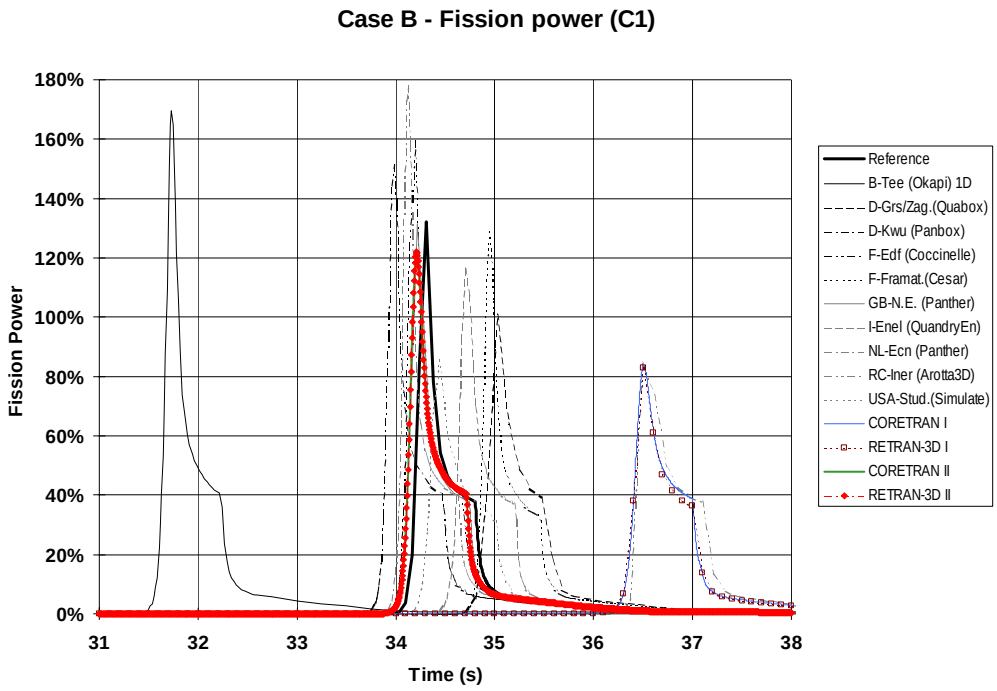

Fig. 5 Transient Case B – Reactor Power

Similarly, the results for case D are shown in Fig.6.

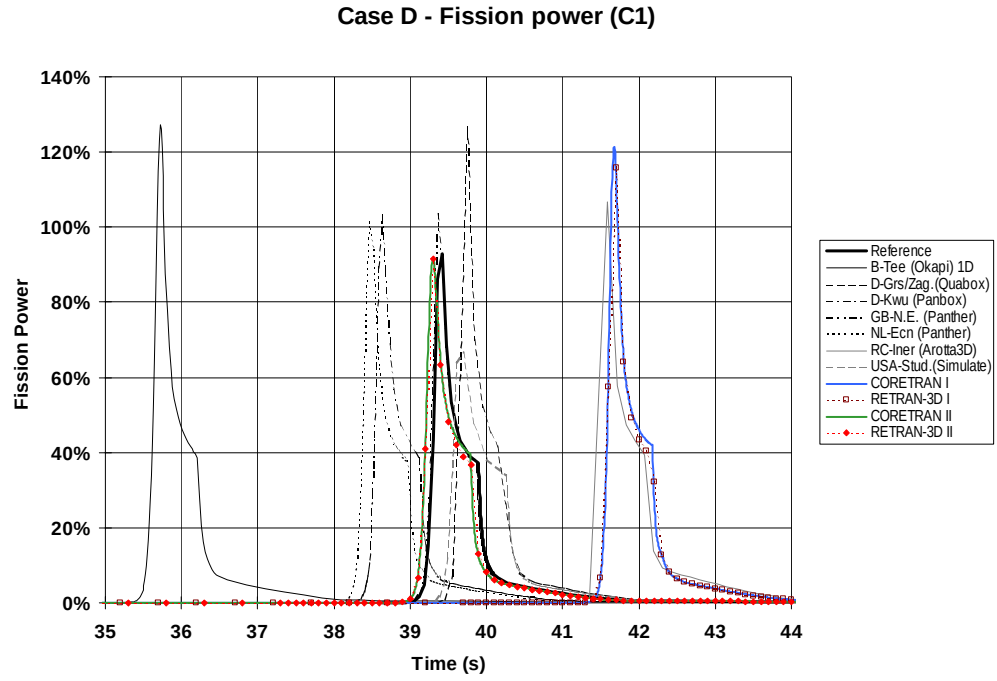

Fig. 6 Transient Case D – Reactor Power

Again, with the linear DCRM, the CORETRAN and RETRAN-3D results are delayed by about 2 s in comparison to most other solutions while the predicted power peak magnitude is now larger. When a non-linear DCRM is used, the delay is reduced and the CORETRAN and RETRAN-3D results agree very well with the previous benchmark solutions. It is also noted that now, the peak magnitude is reduced when a non-linear model is used while the contrary was observed for case B.

A discussion with respect to the influence of the DCRM on the delay and magnitude of the peak power will be presented in the next section.

In addition to the peak power it is important to present and to compare with the previous solutions, the CORETRAN and RETRAN-3D enthalpy deposition. Therefore, the hot pellet enthalpy increase predicted by both codes is shown in Fig 7 for case B and Fig. 8 for case D.

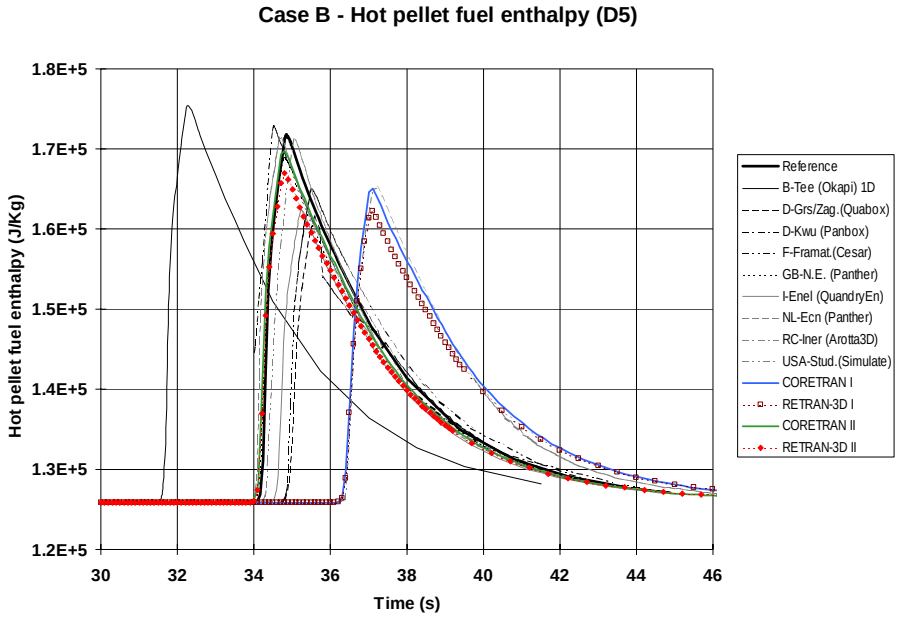

Fig.7 Case B –Hot Pellet Enthalpy

Clearly, from the point of view of maximal inserted enthalpy, the CORETRAN and RETRAN-3D results become more conservative when using a non-linear DCRM model in case B. In case D, the opposite is obtained i.e. the enthalpy increase becomes less conservative with a non-linear DCRM. These results are in-line with the peak power predictions shown above.

A summary of the CORETRAN / RETRAN-3D transient results for the benchmark cases B and D is given in Table 2.

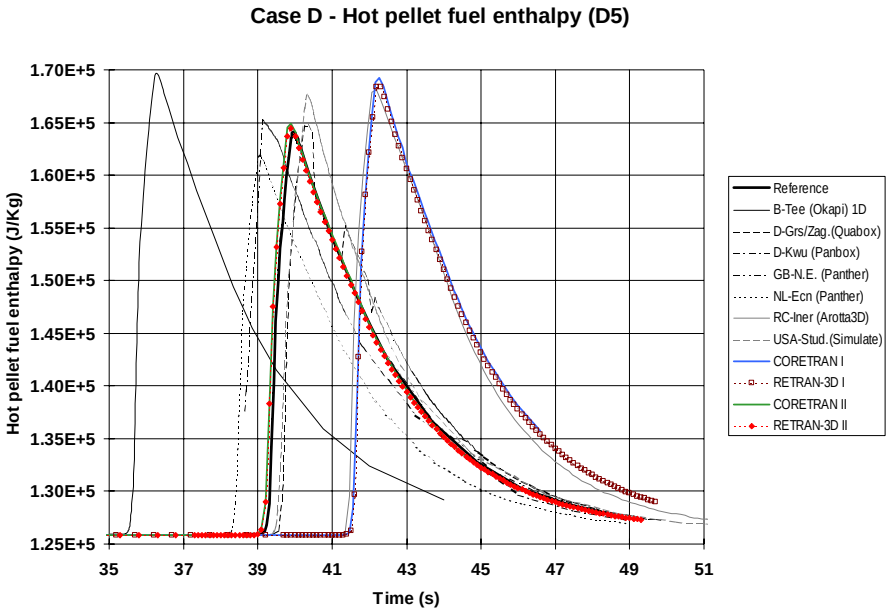

Fig.8 Case D – Hot Pellet Enthalpy

Table 2 – Summary of transient results with CORETRAN / RETRAN –3D

Case	Code	Power Peak		Hot Pellet Enthalpy Increase	
		Peak Time (s)	Peak Magnitude (-)	Peak Time (s)	Enthalpy (J/kg)
B	**Reference**	**34.30**	**1.3480**	**34.85**	**45882**
	Deviations	(s)	(%)	(s)	(%)
	CORETRAN (I / II)	+2.21 / -0.09	-38.0 / -9.6	+2.26 / -0.04	-14.6 / -4.3
	RETRAN-3D (I / II)	+2.20 / -0.10	-38.5 / +10.2	+ 2.25 / -0.05	-20.7 / -10.4
	Previous Solutions STD	*1.20*	*24.5*	*1.28*	*10.6*
D	**Reference**	**39.40**	**0.9685**	**39.95**	**38251**
	Deviations	(s)	(%)	(s)	(%)
	CORETRAN (I / II)	+2.28 / -0.15	+25.3 / -5.4	+2.32 / -0.05	+13.3 / +2.1
	RETRAN-3D (I / II)	+2.30 / -0.10	+19.5 / -5.6	+2.35 / -0.05	+11.1 / +0.9
	Previous Solutions STD	*1.77*	*21.0*	*1.78*	*7.2*

5.3 Discussion

The above results show that when using the nominal linear DCRM in CORETRAN and RETRAN-3D, the predicted power excursion is delayed by around 2 s. Moreover, in case B, such a model leads to an under-estimate of the power peak magnitude, while in case D, the opposite is obtained. In this section, a discussion of the observed delay and the change in the peak magnitude obtained with a non-linear DCRM model is presented.

First, with regard to the delay, it is observed that the DCRM affects the start of the super prompt power excursion phase. If the passage to super-prompt criticality is attained within a given node, a smaller uncontrolled nodal volume will be necessary when using a

non-linear model such as Eq. (2) compared to a linear model as given by Eq. (1). Therefore, the passage to super-prompt criticality will be delayed in a calculation using a linear DCRM. This delay can be shown to be proportional to the ratio of the node height and the withdrawal speed i.e. $\tau \propto \frac{H}{v}$

Hence, if the withdrawal speed is very large or if the axial node height is very small, the delay will be eliminated and the transient solution will be independent of the nature of the DCRM. For fast reactivity transients such as a rod ejection, the form of the DCRM plays practically no role while for slow transients such as analysed here, a certain delay can be expected when using a linear DCRM. Using a finer axial mesh could therefore help to reduce this delay. This explains why an "increased" non-linearity in the DCRM produces an earlier power peak, as obtained in both case B and D (Fig.1 and 2 respectively).

Second, with respect to the peak magnitude, it is noticed that for case B, it is increased when using a non-linear DCRM. For case D, the opposite is obtained i.e. the peak is decreased with a non-linear DCRM. To understand this behaviour, the transient reactivity components for both DCRM calculations are shown in Fig.9 for Case B and Fig. 10 for Case D.

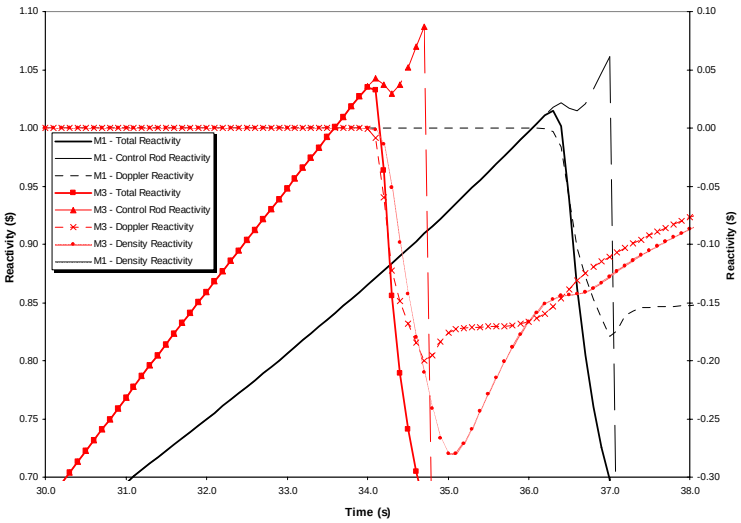

Fig. 9 Case B - Reactivity Components

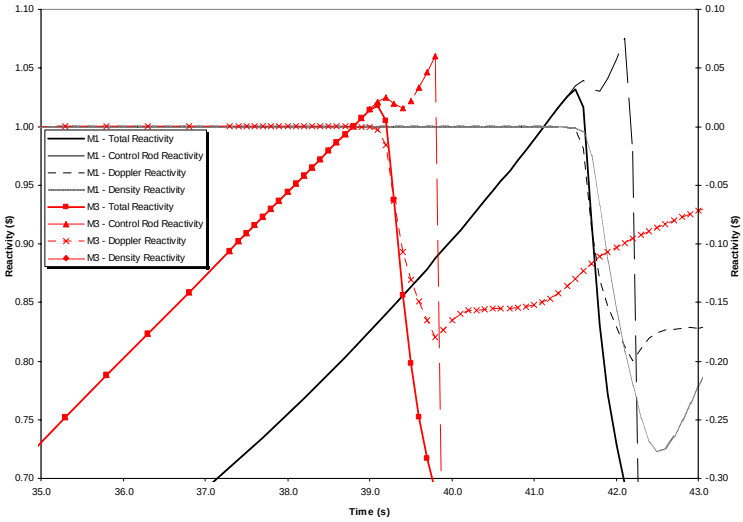

Fig. 10 Case D - Reactivity Components

In these figures, the reversal of the total reactivity corresponds to the start of the increase in the Doppler reactivity. Since the rods are still being withdrawn, the control rod reactivity continues to increase and during this phase, a first dip is observed which corresponds to the start of the reactivity feedback dynamical response. Thereafter, the control rod reactivity insertion further increases until SCRAM. In both cases, it is clearly seen that a non-linear DCRM produces an earlier passage to super-prompt criticality (>1$), emphasizing the delay mentioned previously.

In case B (Fig. 9), it is clearly seen that the control rod reactivity insertion rate after the passage to super-prompt criticality (SPC) is larger with the non-linear DCRM.

The larger control rod reactivity insertion rate produces an “effective delay” in the Doppler response, (since this responds to the integral of the power) which leads to the increased power peak magnitude observed in the previous section. In case D (Fig. 10), it is seen that the opposite occurs i.e. after the passage to SPC, the positive reactivity insertion rate is in fact larger with the linear model.

The reason that a larger rod reactivity insertion rate (after the passage to SPC) is observed with a linear model in case D while the contrary is seen for case B, can be related to Fig. 4a. To do so, the partial rod insertion when SPC is attained is shown in Fig 11a for case B and Fig 11b for case D. Note that in both cases, the SPC is attained within axial node 5 (with a height of 30 cm).

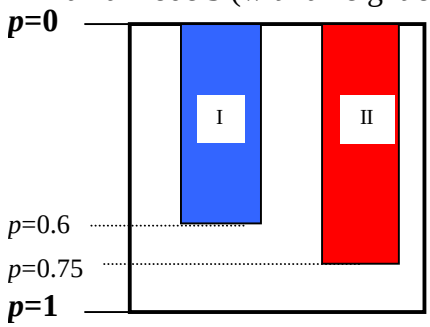

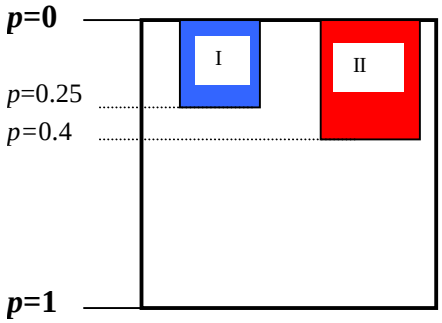

Fig. 11a Case B - Partial Rod Insertion at SPC **Fig. 11b** Case D - Partial Rod Insertion at SPC

In case B, SPC is attained when axial node 5 is to a large extent controlled, which corresponds to Phase I in Fig. 4a. During that phase of the partial node insertion, the reactivity insertion rate is larger with a non-linear model. With such model, the Doppler is therefore delayed and results in a higher power peak magnitude. In case D, because the rod bank worth is lower, the passage to SPC is attained later. As shown by Fig. 11b, it occurs when axial node 5 is nearly fully uncontrolled, which corresponds to Phase III in Fig. 4a. During that phase, the reactivity insertion rate is higher with a linear model and therefore, the Doppler response is now slightly delayed compared to the non-linear DCRM calculation. This explains why in case D, a non-linear model leads to less conservative results.

Finally, it is also interesting to note that the nature of the DCRM has a different impact on the transient flux redistribution in both cases. To illustrate this, the increase in radial factor going from a linear to a non-linear model is shown for case B in Fig. 12a and for Case D in Fig. 12b. As can be seen in Fig. 12a for case B, an increasingly non-linear DCRM induces increasingly higher fluxes towards the peripheral zone, i.e. around the peripheral rod (X=12,Y=12) that is withdrawn, while the flux levels are decreased in a large part of the central core region. On the contrary, for case D shown in Fig. 12b, the peripheral flux is decreased with increasingly non-linear DCRM and the flux redistribution occurs in the central core region. It is hence clear that the DCRM non-linearity causes an opposite flux redistribution behaviour between both transient cases and this of courses influences the core dynamical reactivity response. However, the quantitative impact of the flux redistribution on the core integrated reactivity and hence power response has not been assessed here.

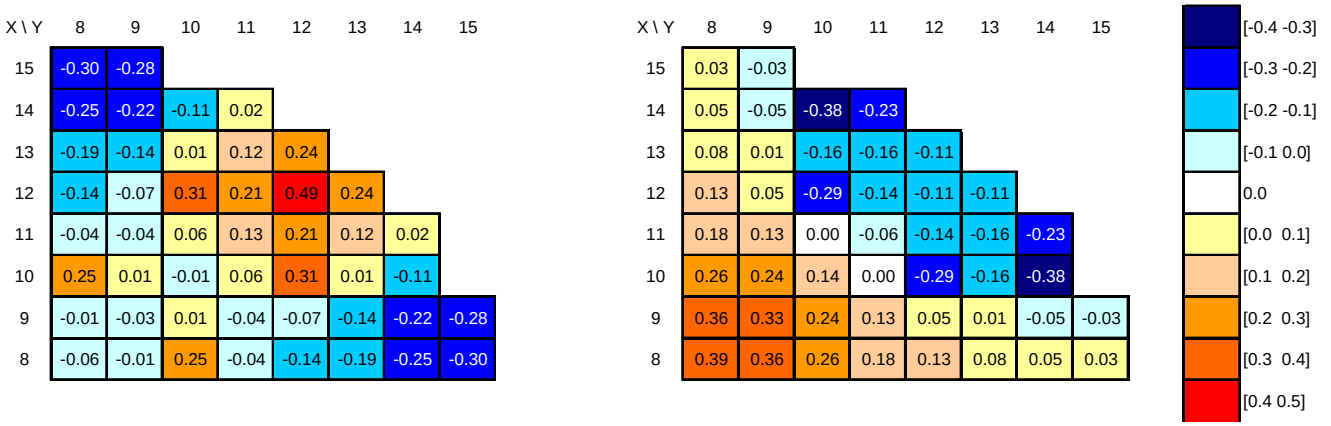

Fig. 12a Case B - Relative increase (%) in radial factors with a non-linear DCRM

Fig. 12b Case D - Relative increase (%) in radial factors with a non-linear DCRM

6 CHANNEL LUMPING IN RETRAN-3D

As mentioned previously, the RETRAN-3D analyses were performed using a full core model (i.e. 2x2 neutronic mesh, 1x1 T/H mesh) taking advantage of the core ¼ symmetry. However, for the future use of RETRAN-3D in coupled 3-D core / thermal-hydraulic system transient analyses of the Swiss LWRs, a lumping of the core T/H channels may be necessary, particularly for large cores.

In (Ferroukhi, 2001b), the impact of the selected channel lumping for an asymmetric rod ejection transient was investigated. Here, a similar study has been performed for the slow reactivity transients analysed in this paper. For that purpose, a lumped RETRAN-3D model using 77 T/H channels (again taking advantage of the core symmetry) was constructed in order to re-analyse transient case B. The lumping scheme is shown in Fig. 13. It is constructed so that the fuel assemblies where the withdrawn rods are located are modelled by individual channels, the fuel assemblies on the core main horizontal and vertical transverse are also modelled as individual channels while the remaining fuel assemblies are grouped according to the initial radial peak factor distribution.

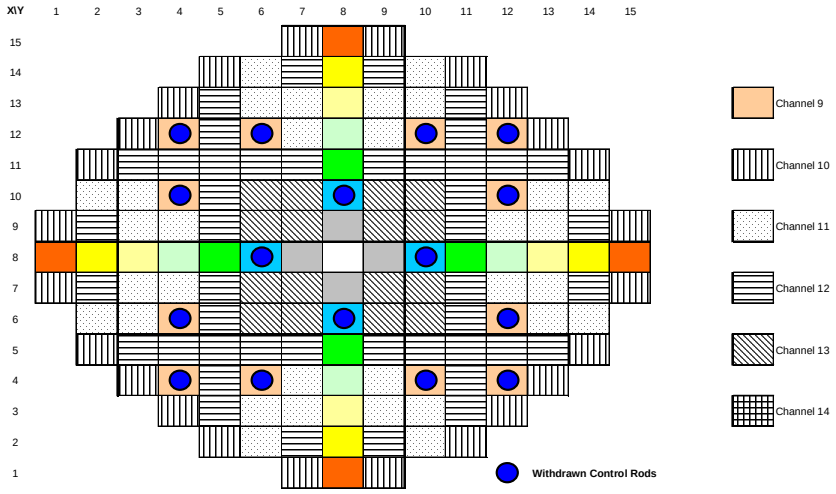

Fig. 13 –RETRAN-3D Lumped 77-T/H Channel Model (1/8 symmetry)

With the above lumping model, the transient case B was re-analysed with RETRAN-3D using the nominal linear DCRM model. The reactor power predicted by RETRAN-3D using this lumping scheme is compared in Fig. 14 to the results obtained using the full core model of the previous section (RETRAN-3D I).

To start, it is noticed that the time of the power peak is unchanged by the channel lumping. This is consistent with the results obtained for a similar study performed for the fast reactivity transient benchmark (Ferroukhi, 2001a). In that analysis it was found that independent of the number of T/H channels used in the lumping scheme, the power peak would occur practically at the same time. In addition, it is here observed that the lumped model predicts a higher power peak magnitude. This is also consistent with the general conclusions made in (Ferroukhi, 2001a). However, for the first benchmark where very fast transients were analysed, it was found that the number of channels had to be reduced to approximately 25 out of 157 to affect the results. For a 37-channel model, the results were identical to the full core model solution.

Here, with a 77-channel model, which is significantly larger than 37, it is observed that the results are already modified in the direction of higher power peak predictions. This suggests that the results are more sensitive to the number of T/H channels for slow reactivity transients than for fast reactivity transients. This can easily be understood considering that an adequate channel lumping should be made so that the transient flux gradients are well separated. If this is not the case, for instance if the lumping is selected so that a T/H homogenisation is made between very hot fuel assemblies and colder fuel channels, a strong impact on the core integrated response can be expected. With such lumping, this impact, which only appears after the passage to SPC in reactivity transients at HZP, would be seen by a delay in the dynamical response of the negative reactivity feedback (mainly Doppler).

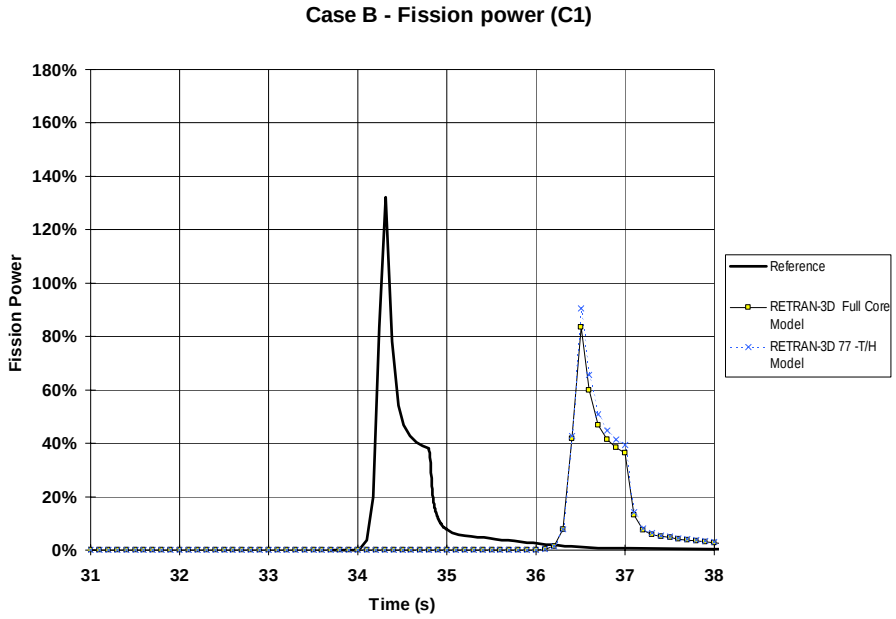

Fig. 14 Case B / Reactor Power – Sensitivity upon RETRAN-3D T/H Channel Lumping

This is what was observed for the fast reactivity transients (Ferroukhi, 2001a). However, because in those cases, the flux gradients were strongest around the ejected rod, the asymmetric nature of the transient allowed for a "simple" T/H grouping. Therefore, provided a sufficient number of channels were modelled individually in this region, the T/H homogenisation in regions further away had very little impact on the results and a similar behaviour to the full core model was observed. However, by reducing the number of T/H channels around the ejected rod, a delay in the Doppler feedback would eventually be introduced causing a longer and more severe power excursion.

For the slow reactivity transient analysed here, the same principle was observed, namely that the lumping introduced a delay in the Doppler feedback which, even though very small, allowed for a longer power excursion. The fact that a delay in the Doppler response is observed with a 77-channel model for this transient, while a 37 channel model gave identical results to a full core model in the rod ejection analysis, illustrates that the choice of the channel lumping for the analysis of a rod bank withdrawal is far more delicate. The reason is that the reactivity insertion occurs simultaneously at several locations in the core, inducing a more complex transient flux redistribution (see Fig. 12a). Therefore, a lumping scheme that is able to capture and separate the transient flux gradients, i.e. so that the T/H homogenisation does not induce a slower response of the core negative feedback, is more difficult to achieve.

One further difference between a rod ejection and a rod group withdrawal is that in the first type of transient, the Doppler reactivity begins to increase after that the entire rod worth has been inserted into the core while in the second type of transient, the increase in Doppler reactivity starts while the rods are still being withdrawn, i.e. while reactivity is being inserted into the core. This means that in the first transient type, the Doppler feedback occurs without any positive reactivity counter-effect. On the other hand, in the second transient type, the Doppler reactivity needs also to compensate for the incremental positive control rod reactivity. Therefore, if the Doppler reaction is delayed,

the additional positive rod reactivity during this delay implies that the Doppler will need to rise to a higher value to attain the negative reactivity contribution necessary to reverse the power. From that point of view, a delay in the Doppler effect has thus a “stronger” impact when the positive reactivity insertion is still going on, i.e. for slow transients.

Finally, it must be emphasised that compared to the STD of the previous solutions (i.e. 21% Table 2), the change in power peak seen in Fig. 14 is very small and the selected lumping scheme can therefore be considered as sufficiently adequate for this particular analysis.

7 CONCLUSIONS

The OECD/NEA benchmark on uncontrolled rod bank withdrawal at hot-zero-power has been analysed with the CORETRAN and RETRAN-3D codes. This work follows a recent analysis performed with both codes of the rod ejection benchmark and forms part of the long-term systematic assessment of these codes against all the OECD/NEA core transient benchmark exercises. As for the previous benchmark analysis, this work shows that the CORETRAN and RETRAN-3D neutronic solutions are consistent both from a static and transient perspective, providing confidence in using the PSI CORETRAN/RETRAN-3D coupling methodology.

When compared to the previous benchmark solutions, the steady-state results of CORETRAN and RETRAN-3D, which reflect mainly the static neutronic solutions in both codes because of the hot-zero-power conditions, are highly satisfactory. From a transient point of view, a generic trend is observed in both codes, namely that the power excursion occurs later (around 2 s) than most other solutions. Moreover, in the transient case (B) where a central and a peripheral rod bank are withdrawn, CORETRAN and RETRAN-3D under predict the power peak, while in case D, where two peripheral rod banks are withdrawn, the contrary is obtained.

Additional calculations showed the delay to be caused by the dynamical control rod model (DCRM), i.e. the model used for the cross-section interpolation for control rods partially inserted within a computational mesh. In the CORETRAN and RETRAN-3D calculations, the current model implemented in both codes and based on a linear interpolation, was used. However, the specifications for this benchmark allowed the use of a more advanced control rod model if available. Therefore, additional calculations were performed with CORETRAN and RETRAN-3D using a non-linear DCRM. It was found that with a non-linear DCRM, the delay in the CORETRAN/RETRAN-3D solutions could be eliminated and that the results (power peak and enthalpy increase) were now in excellent agreement with the previous benchmark solutions. It was also found that depending on the location of the reactivity insertion and particularly, on the worth of the involved rod banks, a non-linear model could lead to an increase or decrease in the magnitude of the peak power.

It must be noted that this problem was not encountered when analysing the rod ejection benchmark since the ejection speed was so high that any delay introduced by the control rod model would be eliminated. For slow reactivity transients on the other hand, because of the low withdrawal speed, a linear model introduces a delay which can significantly affect the results. The main conclusion from this work is hence that a more advanced physically based DCRM should be developed and implemented in

CORETRAN and RETRAN-3D in order to allow for a correct analysis of both fast and slow transients. If the current linear DCRM is used, the analysis with CORETRAN / RETRAN-3D of transients involving a slow movement of control rods should be performed with very small axial computational meshes.

Finally, similar to that for the rod ejection benchmark, a sensitivity analysis to the thermal-hydraulic channel lumping in RETRAN-3D was performed. It is found that for slow reactivity transients such as analysed here, i.e. where the reactivity insertion occurs simultaneously in several core regions, an adequate channel lumping (i.e. so that the flux gradients are well captured and separated) will require a higher number of individual T/H channels than for the analysis of a "local" event such as a single rod ejection.

8 ACKNOWLEDGEMENTS

This work was partly funded by the Swiss Federal Nuclear Safety Inspectorate (HSK[1]) and the Swiss Federal Office of Energy (BFE[2]).

[1] Hauptabteilung für die Sicherheit der Kernanlagen
[2] Bundesamt für Energie

9 REFERENCES

Bennewitz, F., Finnemann, H., Wagner, M.R. Higher Order Corrections in Nodal Calculations. Trans. Am.Nucl.Soc., **22**, 250-251, 1975

Eisenhart, L.D. ARROTTA-01 – An Advanced Rapid Reactor Operational Transient Analysis Computer Code – Volume 1: Theory and Numerics. EPRI, NP-7375, Volume 1, October 1991

Ferroukhi, H., Coddington, P. Three-Dimensional Space-Time Kinetic Analysis with CORETRAN and RETRAN-3D of the NEACRP PWR Rod Ejection Benchmark . PSI Scientific Report 2000, Volume IV, 2001a

Ferroukhi, H., Coddington, P. Analysis and Sensitivity Studies with CORETRAN and RETRAN-3D of the NEACRP PWR Rod Ejection Benchmark. Proc. Int. Conf. On Nuclear Engineering ICONE-9, Nice, April 2001b

Ferroukhi, H., Coddington, P. Analysis with CORETRAN and RETRAN-3D of the OECD / NEA PWR Benchmark on Uncontrolled Rods Withdrawal at Zero Power. PSI Internal Report, Paul Scherrer Institut TM-41-01-10, 2001c

Finnemann, H., Bauer, H., Galati, A.,Martinelli, R. Results of LWR Core Transient Benchmarks. NEA/NSC/DOC(93)25, October 1993

Finnemann, H., Galati, A. NEACRP 3-D LWR Core Transient Benchmark – Final Specifications. NEACRP-L-335,Rev. 1, January 1992

Fraikin, R., Finnemann, H. NEA-NSC 3-D/1-D PWR Core Transient Benchmark Uncontrolled Withdrawal of Control Rods at Zero Power. NEA/NSC/DOC(93),Rev.1, September 1993

Fraikin, R. PWR Benchmark on Uncontrolled Rods Withdrawal at Zero Power – Final Report. NEA/NSC/DOC(96)20, September 1997

Scandpower . RAMONA-3 user's Manual . Rev13., October 1996

Smith, K. An Analytical Nodal Method for Solving the Two-Group, Multidimensional, static and Transient Neutron Diffusion Equation. Thesis. MIT, 1979

NOMENCLATURE

Σ	Actual Macroscopic Nodal Cross-Section	(cm^{-1})
p	Rod Nodal Insertion Fraction	(-)
$f(p)$	Interpolation Function for Partial Rod Insertion	(-)
b	Non-linearity Parameter for the Interpolation Function $f(p)$	(-)
τ	Delay in passage to super-prompt criticality	(s)
H	Axial Node height	(cm)
v	Rod Withdrawal Speed	(cm/s)

Subscripts

C	Controlled Node
U	Uncontrolled Node
f,2	*Thermal Fission*
a,2	Thermal Absorption